Editor's Focus

A unified thermodynamic picture for the glass transition and liquid fragility

Lijian Song[1,2], Meng Gao[1,2], Juntao Huo[1,2], Li-Min Wang[3,4*], Yuanzheng Yue[5*],
and Jun-Qiang Wang[1,2*]

[1] *CAS Key Laboratory of Magnetic Materials and Devices, and Zhejiang Province Key Laboratory of Magnetic Materials and Application Technology, Ningbo Institute of Materials Technology and Engineering, Chinese Academy of Sciences, Ningbo 315201, China*

[2] *Center of Materials Science and Optoelectronics Engineering, University of Chinese Academy of Sciences, Beijing 100049, China*

[3] *State Key Laboratory of Metastable Materials Science and Technology, College of Materials Science and Engineering, Yanshan University, Qinhuangdao 066004, China*

[4] *School of Materials Science and Engineering, Hebei University of Technology, Tianjin 300401, China*

[5] *Department of Chemistry and Bioscience, Aalborg University, Aalborg 9220, Denmark*

Glass transition is a reversible transition that occurs in most amorphous materials. However, the nature of glass transition remains far from being clarified. A key to understand the glass transition is to clarify what determines the glass transition temperature (T_g) and liquid fragility (m). Here the glass transition thermodynamics for 150 different glass-forming systems are studied statistically. It is found that the activation characters in the energy landscape are crucial to precisely portray the glass transition and, in particular, both the activation free energy (G^*) and the activation entropy (S^*) play critical roles. G^* determines T_g, $T_g=G^*/290+25.5$, while S^* determines m, $m=S^*/R\ln10+15$, where R is the gas constant. Based on the Boltzmann definition of entropy, the fragility is an indication of the number of the degeneracy of the evolution paths. This explains why the nano-confined, low-dimension or high-pressured glasses exhibit stronger characteristics, which has been a puzzling phenomenon for a long time.

glass transition, fragility, activation entropy, activation free energy

PACS number(s): 61.43.Dq, 64.70.pf, 81.05.Kf

1 Introduction

Glass can form various kinds of materials, including organic matter [1], inorganic compounds [2], alloys [3], and metal-organic frameworks [4], with only several exceptions like liquid helium and liquid nitrogen. The glass-liquid transition

temperature (T_g) [5-10] is a measure of the thermal stability of glasses, i.e., the temperature limit of its elastic solid state, above which it transforms into a viscous liquid. Thus, it has been a long-lasting curiosity to design glasses with higher T_g and to understand what determines T_g. It is reported that T_g is closely related to the bond strength, elastic modulus, and topological constraints [11-13]. A series of Ir- and Os-based bulk metallic glasses with very high T_g have been designed in this strategy [3,14]. Ediger's group [1,15] proposed fabri-

cating ultrastable glasses with enhanced T_g by increasing the atomic bonding strength by surficial fast relaxation. Despite these experimental advancements in designing glasses with high T_g, the thermodynamic origin and kinetics of glass transition are far less understood.

The glass transition is a kinetic process that depends on the heating rate [7,16]. The rate dependence of T_g is closely related to the fragility (m) of glass-forming liquids, which is a technical parameter defined by Angell [17] to quantify the non-Arrhenius behavior of a glass-forming liquid. The glasses with similar T_g may have distinct m. For example, T_g of the $Fe_{79}Si_{10}B_{11}$ metallic glass and GeO_2 glass are the same, i.e., 818 K, but their fragilities are significantly different, i.e., m=117 for $Fe_{79}Si_{10}B_{11}$ [18,19] versus m=20 for GeO_2 [20], respectively. The m ranges from 15 to 214 for various glass-forming liquids [21,22]. The liquids with a small m are usually called "strong" liquids, whereas those with a large m are called "fragile" liquids. The physical properties of glasses have close relations with their m values. For example, it is positively related to Poisson's ratio and plasticity [23]. A strong liquid usually exhibits higher glass-forming ability [24,25] and a higher stability against crystallization [26,27]. Even though the technical definition for m is clear and it has close correlations with other properties of glasses, the thermodynamic and structural origins of the liquid fragility remain less known.

In this work, based on the absolute reaction rate theory we calculate the thermodynamic parameters that characterize the glass transition of various glass systems, e.g., the activation enthalpy H^*, the activation free energy G^*, and the activation entropy S^*. We investigate the correlation between T_g and G^*, as well as the relation between S^* and the liquid fragility, so that the topographic complexity of potential energy landscape (PEL) can be revealed. Finally, we give experimental evaluations on the PEL of glass-forming liquids.

2   Methods

The two-state system is usually applied to describe the reaction kinetics. For example, the reaction rate is given as $k' \propto \exp\left(-\dfrac{H^*}{RT}\right)$, where H^* is the reaction barrier, R is gas constant, and T is temperature. For glass transition, it is a process entailing multiple barriers. If there are Ω transition states/evolution paths with an averaged barrier of H^*, a factor of Ω should be multiplied with the single-barrier reaction rate,

$$k' \propto \exp\left(-\frac{H^*}{RT}\right) \times \Omega = \exp\left(-\frac{H^*}{RT}\right) \times \exp(\ln\Omega).$$

Note that Ω is also regarded as the thermodynamic probability of the state or the number of different ways in which a particular configuration can be achieved. Here, we define an activation entropy S^* based on the Boltzmann definition of entropy:

$$S^* = R\ln\Omega. \tag{1}$$

Then, it gives that

$$k' \propto \exp\left(-\frac{H^*}{RT}\right) \times \exp\left(\frac{S^*}{R}\right), \tag{2}$$

which is consistent with the absolute reaction rate theory (ART, also known as transition state theory, TST) [28-30],

$$-\frac{d\sigma}{dt} = \frac{\kappa k_B T}{h_P}\exp\left(-\frac{G^*}{RT}\right)\sigma = \frac{\kappa k_B T}{h_P}\exp\left(-\frac{H^*}{RT}\right)\exp\left(\frac{S^*}{R}\right)\sigma,$$

where σ is the internal stress that is frozen-in during glass formation and is released during glass transition to a supercooled liquid state, t is time, κ is the tunneling transmission coefficient with $\kappa=1+h_P\omega/24k_BT$, ω is the angular frequency, h_P is the Planck constant. $G^*=H^*-T_gS^*$ is activation free energy. H^* represents a statistically averaged barrier for the transition states. It is linearly related to the kinetic energy barrier (E^*) determined in the Kissinger equation, $H^*=E^*-RT$ (see Supporting Information or refs. [30,31]). During glass transition, the $d\sigma/dt$ reaches the maximum [32]. It gives $d(d\sigma/dt)/dt=0$,

$$\ln\frac{R_h}{T^3} = \ln\frac{\kappa k_B R}{h_P} + \ln\frac{1}{H^*} + \frac{S^*}{R} - \frac{H^*}{RT}, \tag{3}$$

where R_h is the heating rate. From eq. (3), the thermodynamic parameters (H^*, S^*) can be obtained by measuring the heating rate dependence of T_g.

3   Results

3.1   The kinetics characters of glass transition temperature

Figure 1 shows the relation between H^* and T_g for 150 different glass-forming systems, including metals, oxides, chalcogenides, molecules, and polymers. The T_g values of these systems range from 100 to 1000 K. In Figure 1(a), it is seen that the activation enthalpy H^* increases along with T_g in an approximately linear fashion, where the data are rather scattered. In Figure 1(b), there is no clear relation between S^* and T_g. However, interestingly, when plotting the activation free energy G^* ($=H^*-T_gS^*$) against T_g, we have observed a striking linear relation for those glass systems as shown in Figure 1(c). This suggests that T_g is intimately associated with the activation free energy for glass transition. The slope of the linear relation is found to be about G^*/T_g= 290 J mol^{-1} K^{-1}. According to the elastic model [11,12,33,34], G^* should be proportional to the atomic bonding strength.

Another intriguing point in Figure 1(c) is that there is an intercept for the linear relation at about T=25.5 K at G^*=0. This implies that the lowest glass transition temperature should be above 25.5 K. This is supported by the experi-
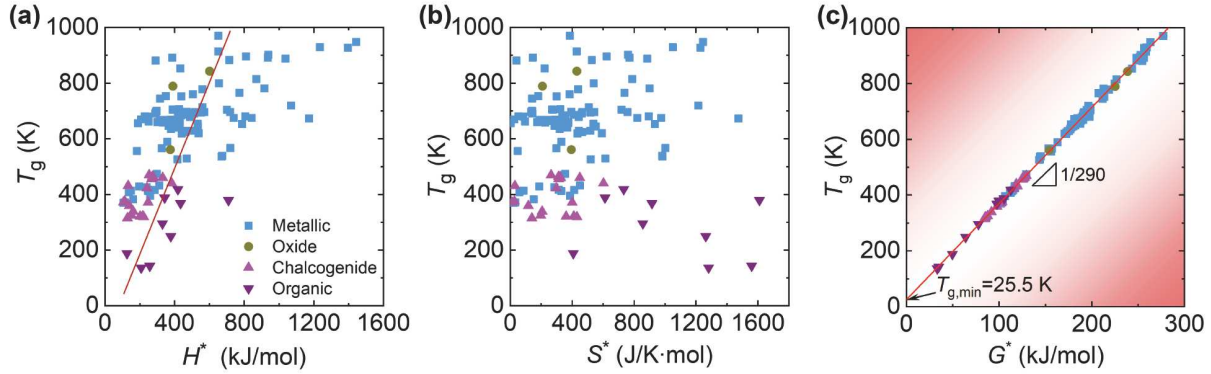
Figure 1 (Color online) The thermodynamic parameters versus glass transition temperature T_g for different types of glasses. (a) The activation enthalpy H^* versus T_g for metallic glasses, organic glasses, oxide glasses, and chalcogenide glasses. (b) The activation entropy S^* versus T_g. (c) The activation free energy G^* versus T_g. The linear fitting yields a slope of 1/290 and an intercept of 25.5 K (lower limit of T_g).

mental results. The lowest T_g measured in experiments is 45.5 K for the glassy propane prepared by vapor deposition [35], while the second lowest T_g is about 56 K obtained in glassy propene [36] and propylene [37]. The vapor-deposited amorphous ethane is expected to have a T_g around 25.5 K, but it crystallizes at 23.9 K without exhibiting glass transition [35,37]. The correlation between boiling temperature and T_g also suggests that T_g may have a lower limit [38]. The missing of glass transition below 25.5 K is attributed to the quantum tunneling effect [39-41]. At low temperatures, the tunneling transmission coefficient $\kappa=1+h_P\omega/24k_BT$ becomes large enough [39,40], which allows atoms to penetrate the small thermodynamic barrier of glasses with T_g lower than 25.5 K. This explains why liquid nitrogen and liquid helium cannot be vitrified.

To examine the universality of the linear relation between G^* and T_g, the T_g values are compared between poly-amorphisms in metallic glasses and between the as-cooled and the heavily-relaxed glasses as shown in Figure 2. It is seen in Figure 2(a) that the annealed glasses display higher T_g than the as-quenched glasses. For NbNiZrTiCu high-entropy polyamorphic metallic glass (MG) [42], T_g increases from 672 K for the as-cooled sample to 732 K for the relaxed one, and correspondingly, G^* increases from 190 to 210 kJ/mol (Figure 2(a)). For CuZr-based MGs, T_g increases from 651 to 685 K when G^* increases from 186 to 190 kJ/mol (Figure 2(b)). T_g and G^* values for Zr-based MGs were calculated based on the previously reported data [43]. It is seen that these values follow the same linear trend in Figure 2(b). This implies that the linear relationship between G^* and T_g is universal, i.e., independent of the type of chemical bonds and the polyamorphism of glasses.

3.2 Fragility and activation entropy

In Boltzmann definition of S^* in eq. (1), a larger S^* denotes more evolution paths or transition states (larger Ω). The Ω

reflects the degree of complexity in the potential energy landscape (PEL). In the PEL theory, the complexity of the energy landscape is thought to be related to the fragility index m of the glass-forming liquid [7,46,47]. This motivates us to explore the relationship between S^* and m. Strikingly and definitely, Figure 3(a) shows that m increases linearly with S^* with a slop of about 0.050 ± 0.03 J^{-1} mol K, being consistent with the PEL theory [7,46]. The intercept (S^*=0) of the linear relation occurs at about m=15, i.e., at the lower limit of the liquid fragility, indicating that the activation entropy of the strongest glass-forming liquid (e.g., silica [20,48]) is close to zero.

The underlying physical mechanism for the linear relationship between m and S^* is studied based on the Mauro-Yue-Ellison-Gupta-Allan (MYEGA) model [21],

$$\log_{10}\eta(T) = \log_{10}\eta_\infty + (12 - \log_{10}\eta_\infty)$$
$$\cdot \frac{T_g}{T}\exp\left[\left(\frac{m}{12-\log_{10}\eta_\infty}-1\right)\left(\frac{T_g}{T}-1\right)\right].$$

The fragility index $m = \dfrac{d\log_{10}\eta(T)}{d(T_g/T)}$ and the activation energy E^* can be linked by the temperature dependence of viscosity [49,50]: $E^*=mRT_g\ln10$. Given $H^*=E^*-RT$ and the thermodynamic relation

$$S^* = \int \frac{dH^*/dT}{T}dT = (m-m_{min})R\ln10,$$

it gives

$$m = S^*/R\ln10 + m_{min}, \tag{4}$$

where m_{min}=15 [51,52]. It is worth noting that the Volgel-Fulcher-Tammann (VFT) equation yields a similar relationship (eq. (4)) with that from the MYEGA model (see Supporting Information).

In Figure 3(a), the linear fitting with a slope of $1/R\ln10$=0.052 agrees well with the experimental data. The scattering of the experimental data should be attributed to the
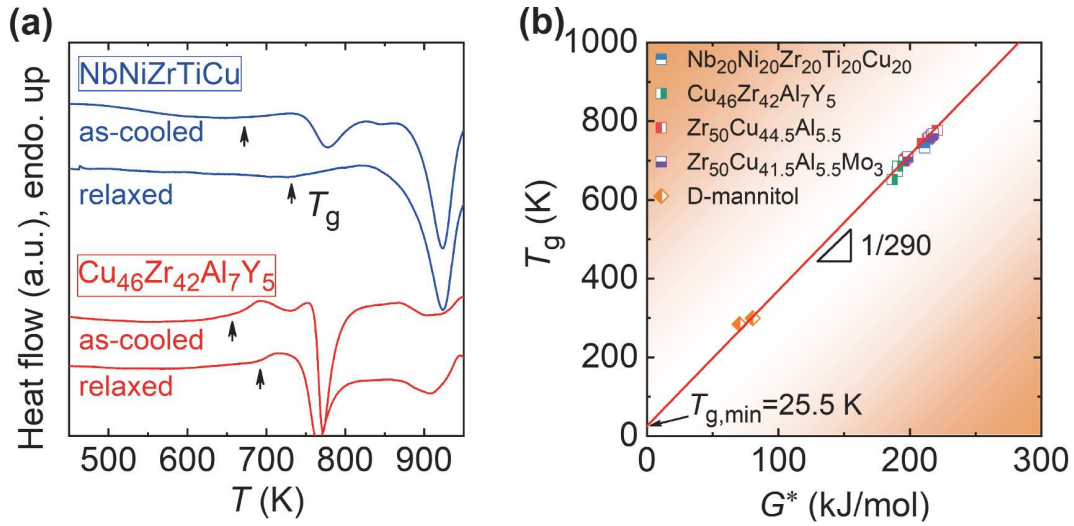
Figure 2 (Color online) The calorimetric glass transition in polyamorphic metallic glasses and its relation to the activation free energy G^*. (a) The representative DSC curves for both the as-cooled metallic glass and the relaxed high-stable glass with higher T_g. The upper two traces are obtained from high-entropy NbNiZrTiCu glass. The lower two traces are from $Cu_{46}Zr_{42}Al_7Y_5$ glass. (b) The activation free energy (G^*) versus T_g for the polyamorphic glasses. The data for the relaxed $Zr_{50}Cu_{44.5}Al_{5.5}$ and $Zr_{50}Cu_{41.5}Al_{5.5}Mo_3$ glasses are taken from ref. [43], and the data for D-mannitol glasses are from refs. [44,45].
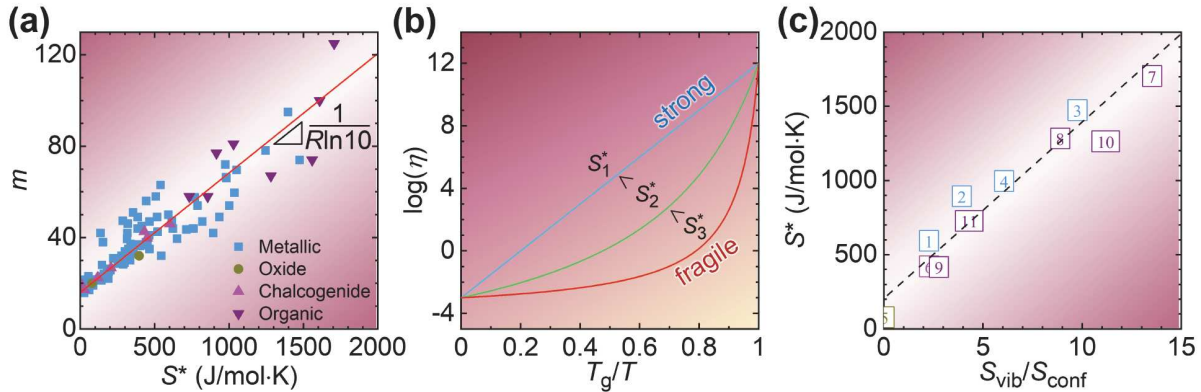

Figure 3 (Color online) The correlation between fragility and activation entropy. (a) Fragility m versus the activation entropy S^*, which exhibits a linear relationship with a slope of $1/R\ln10$ (R is gas constant). (b) The schematic Angell plot of viscosity η versus T_g/T. The strong supercooled liquid has a smaller activation entropy than the fragile supercooled liquids. (c) The activation entropy S^* is correlated with the ratio between vibrational entropy S_{vib} and configurational entropy S_{conf}. 1, $Pd_{40}Ni_{40}P_{20}$; 2, $Zr_{55}Cu_{30}Al_{10}Ni_5$; 3, $Cu_{50}Zr_{50}$; 4, $Cu_{46}Zr_{46}Al_8$; 5, SiO_2; 6, $Ge_{20}Se_{80}$; 7, Toluene; 8, Ethylbenzene; 9, 1-Butene; 10, OTP; 11, 3-Bromopentane.

experimental errors of different measurements. Combining eqs. (1) and (4), we obtain the following equation, by which the number of the evolution paths can be estimated:

$$m = \log_{10}\Omega + 15. \tag{5}$$

Combining the relations $H^*=E^*-RT_g$, $E^*=mRT_g\ln10$ and $H^*=G^*+T_gS^*$, we obtain the relation $G^*=mRT_g\ln10-RT_g-T_gS^*$, leading to the equation: $G^*/T_g=R(m_{min}\ln10-1)$. The slope G^*/T_g in Figure 1(c) determines the smallest fragility to be $m_{min}=14.6\pm0.4$, which is consistent with that reported previously [51]. To the best of our knowledge, this relation is the first to quantify the relation between dynamic liquid fragility and the thermodynamic probability of states (or the number of evolution paths of configurational states), as

shown in Figure 3(b).

The number of the transition states Ω during glass transition should be related to the atomic/molecular motions, i.e., involve vibrational, translational, and rotating motions that can provide kinetic energy for transitions. This suggests that the activation entropy S^* is positively related to vibrational entropy S_{vib}. When considering the degeneracy of transition states, S^* should be inversely related to the configurational entropy S_c. The S_{vib} can be obtained by measuring the vibrational density of states in experiments [53,54]. The ratio of S_{vib}/S_c represents the degeneracy of transition states over static configuration. Figure 3(c) confirms the linear relation between S^* and S_{vib}/S_c, which is also in line with refs. [55,56].

It should be mentioned that the present method is much easier to determine entropy compared with the neutron anelastic scattering experiments [53,54]. Either S_c or S^* can be obtained from calorimetry measurements. The S_c can be calculated based on the heat capacity, while S^* can be calculated based on the heating rate dependence of T_g.

To gain deeper insights into glass transition, the roles of H^*, S^*, and G^* in the glass forming process are illustrated in Figure 4 based on the PEL. In PEL, H^* represents the effective barrier for glass transition, which is a statistically averaged value of a big number of single barriers. It was generally accepted that a higher H^* yields a higher T_g. Our
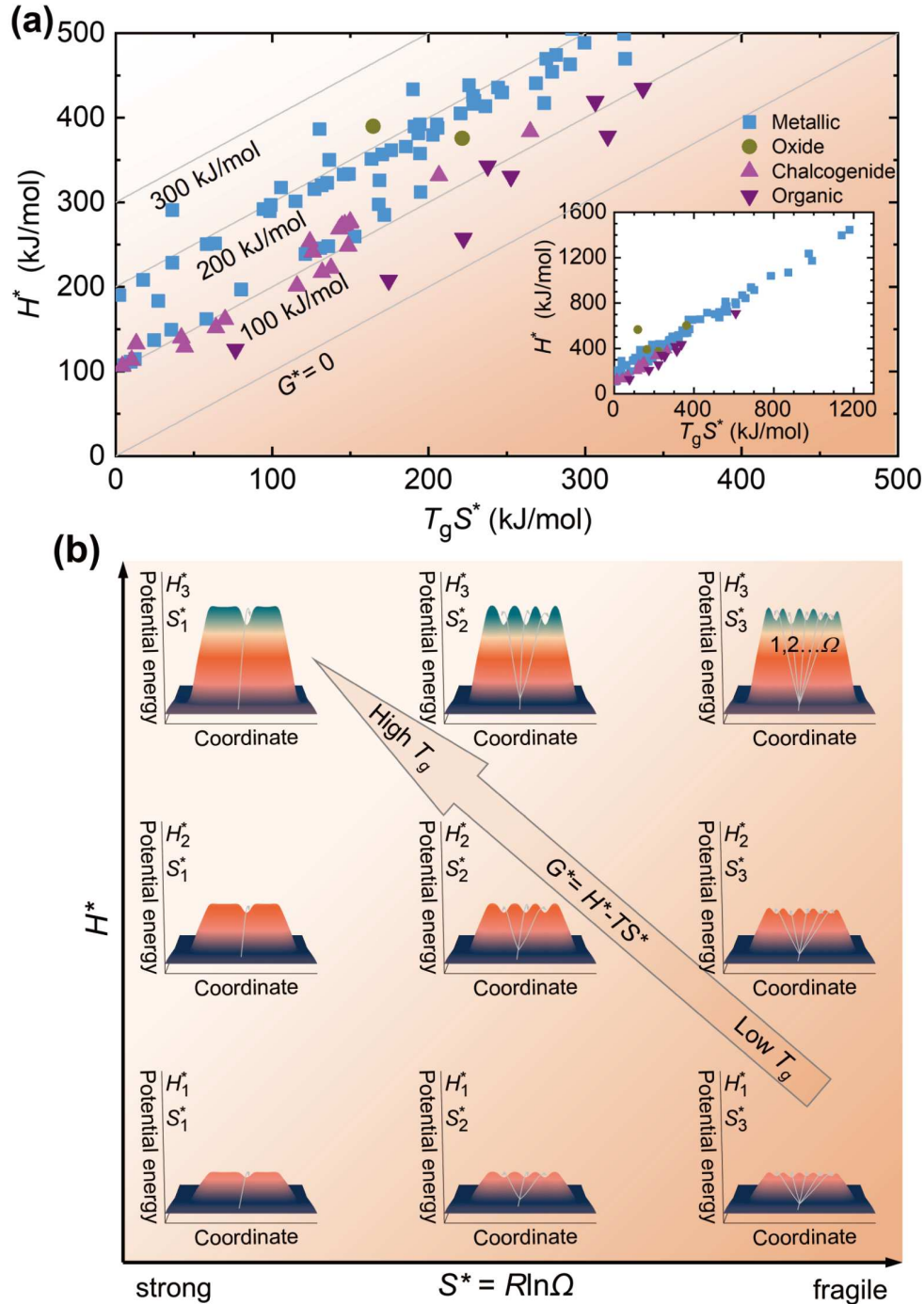

Figure 4 (Color online) The kinetic nature of glass transition. (a) The relationship between activation enthalpy and activation entropy. The contour lines of different $G^*=H^*-TS^*$ represent different T_g. Inset is the relationship between activation enthalpy and activation entropy for all samples. (b) Schematic potential energy landscape with different activation enthalpy H^*, activation entropy S^*, and activation free energy G^*. H^* represents the barrier height, $H_1^* < H_2^* < H_3^*$. S^* represents the number/degeneracy (Ω) of transition states with $S^*=R\ln\Omega$, $S_1^* < S_2^* < S_3^*$. S^* determines the fragility of glass forming liquid. G^* determines the T_g.

results demonstrate that this effective barrier will decrease by $-TS^*$ if there are many evolution paths (number is Ω). This yields a linear relation between G^* and T_g. As shown in Figure 4(a), H^* does not show linear relation with S^*, which breaks the Meyer-Neldel rule [57,58]. The contour lines of different $G^* = H^* - T_g S^*$ represent different T_g. As schematically illustrated in Figure 4(b), S^* that is determined by the number of evolution paths determines the fragility of glass-forming liquid, while G^* determines T_g.

4   Discussion

For glasses composed of atoms and simple molecules, the evolution paths are mainly composed of vibrational and translational motions. The degree of atomic motion freedom in 6 dimensions gives the Ω value of $(6.02 \times 10^{23})^6$, from which the liquid fragility is estimated to be 142.7. However, there is strong atomic bonding between each central atom and its nearest-neighbors or medium-range order range. The amount of the evolution paths or the liquid fragility should be smaller if stronger atomic bonds are involved in glass systems, as recently found by experiments [59].

For a glass-forming system with a rigid network, e.g., for the case of molten silica, its atom-evolution paths are depressed, and hence, its fragility approaches the lower limit. The molecular glass-forming liquids feature larger fragility than other systems for the following two reasons. First, the molecules exhibit rotational motions besides the vibrational and translational motions. Second, more low-frequency vibrations are generated in both liquids and solids, being driven by the increased soft/floppy modes. The degree of atomic motion freedom in 9 dimensions (3×vibrations, 3×translations and 3×rotations) gives the Ω value of $(6.02 \times 10^{23})^9$. These dynamic motions give an upper limit of the fragility, i.e., $m_{max} = \log_{10}(6.02 \times 10^{23})^9 + 15 = 229$, which is slightly higher than the upper limit of $m \sim 175$ derived from the thermodynamic consideration [60] and the most fragile simulated silicon melt ($m \sim 200$) [61] and polyetherimide ($m = 214$) [22].

It was found that liquid fragility is correlated with the heterogeneities of supercooled liquids and glasses [20,62]. It is also challenging to predict the stress relaxation behavior owing to the complex evolution of heterogeneity [63]. The mathematical definitions for activation entropy in eq. (1) and for fragility in eq. (5) based on the degeneracy of transition states may be helpful for establishing quantitative evaluation for heterogeneity in future.

The linear correlation between liquid fragility and activation entropy provides a crucial key to understanding the connection between the dynamics and the thermodynamics in glass-forming liquids. Furthermore, it also allows us to explore the origin of the dependence of glass forming ability on liquid fragility. In detail, the higher the number of evolution paths in a liquid system, the higher the probability for the system to lose its stability of the disordered structure, and the lower the glass forming ability. This statement is consistent with previous observations [17,64]. Considering the liquid-glass inheritance [65], the glass derived from a fragile liquid is easier to deform, giving a higher Poisson's ratio [23] compared with a strong liquid.

It has been a long-lasting puzzling phenomenon that the nano-confined, low-dimension, or high-pressured glasses usually exhibit smaller fragility compared with bulk glasses under ambient pressure [44,66,67]. The correlation between fragility m and $S^* = R \ln \Omega$ suggests that the nano-confinement, decrease in dimension or high-pressure can decrease the number of evolution paths. Thus, S^* provides an important route to design glasses with desirable properties.

The linear relation between G^* and T_g can be applied to estimate the free volume during glass transition. According to Hirai and Eyring [68], the fluidity of liquids is proportional to the probability for the atom to be adjacent to a hole and also to the rate at which it jumps into the hole. Based on this model [68], the shear viscosity of liquids can be expressed as $\eta_s = \dfrac{nN_0}{N_h} \dfrac{h_P}{v_0} \exp\left(\dfrac{H^* - TS^*}{RT}\right)$, where v_0 is the volume of atom ($\approx 2 \times 10^{-29}$ m^3) [11,69], n is the ratio between the volume of atoms and that of holes, N_0 and N_h are the numbers of atoms and holes, respectively. Thus, the fraction (N_h/nN_0) of the hole volume (or the free volume) is estimated to be about ~4.7 % at T_g, which is consistent with ref. [70].

5   Conclusions

In summary, we studied the activation free energy and activation entropy of the glass transition for various types of glasses based on the absolute reaction rate theory. The universal linear relations between thermodynamic and kinetic parameters for glass transition were discovered, i.e., the relations between the activation free energy G^* and T_g, and between the activation entropy S^* and the fragility index m of glass forming liquids. The linear relationship between G^* and T_g suggests a lower T_g limit of about 25.5 K, below which the quantum tunneling effect dominates and the statistical thermodynamic barrier for glass formation is negligible. According to the definition of the Boltzmann definition of entropy, we reveal that the liquid fragility is intimately correlated with the number of evolution paths, $m = \log_{10} \Omega + 15$. Our present work enables a quantitative analysis of glass transition in terms of the potential energy landscape and reveals the microscopic origin of liquid fragility.

Supporting Information

The supporting information is available online at http://tech.scichina.com and https://link.springer.com. The supporting materials are published as submitted, without typesetting or editing. The responsibility for scientific accuracy and content remains entirely with the authors.

1 S. F. Swallen, K. L. Kearns, M. K. Mapes, Y. S. Kim, R. J. McMahon, M. D. Ediger, T. Wu, L. Yu, and S. Satija, Science **315**, 353 (2007).
2 G. N. Greaves, and S. Sen, Adv. Phys. **56**, 1 (2007).
3 M. X. Li, S. F. Zhao, Z. Lu, A. Hirata, P. Wen, H. Y. Bai, M. W. Chen, J. Schroers, Y. H. Liu, and W. H. Wang, Nature **569**, 99 (2019).
4 R. S. K. Madsen, A. Qiao, J. Sen, I. Hung, K. Chen, Z. Gan, S. Sen, and Y. Yue, Science **367**, 1473 (2020).
5 P. Charbonneau, A. Ikeda, G. Parisi, and F. Zamponi, Phys. Rev. Lett. **107**, 185702 (2011).
6 H. B. Yu, R. Richert, R. Maaß, and K. Samwer, Phys. Rev. Lett. **115**, 135701 (2015).
7 P. G. Debenedetti, and F. H. Stillinger, Nature **410**, 259 (2001).
8 S. Torquato, Nature **405**, 521 (2000).
9 S. Sastry, Nature **409**, 164 (2001).
10 Y. Yue, and C. A. Angell, Nature **427**, 717 (2004).
11 J. Q. Wang, W. H. Wang, Y. H. Liu, and H. Y. Bai, Phys. Rev. B **83**, 012201 (2011).
12 W. H. Wang, Prog. Mater. Sci. **57**, 487 (2012).
13 C. Hermansen, J. C. Mauro, and Y. Yue, J. Chem. Phys. **140**, 154501 (2014).
14 J. Bi, X. Wei, X. Liu, R. Li, R. Xiao, and T. Zhang, Scripta Mater. **228**, 115336 (2023).
15 K. J. Dawson, K. L. Kearns, L. Yu, W. Steffen, and M. D. Ediger, Proc. Natl. Acad. Sci. USA **106**, 15165 (2009).
16 M. S. Beasley, C. Bishop, B. J. Kasting, and M. D. Ediger, J. Phys. Chem. Lett. **10**, 4069 (2019).
17 C. A. Angell, Science **267**, 1924 (1995).
18 B. Dong, S. Zhou, J. Qin, Y. Li, H. Chen, and Y. Wang, Prog. Nat. Sci.-Mater. Int. **28**, 696 (2018).
19 C. Zhang, Q. Chi, J. Zhang, Y. Dong, A. He, X. Zhang, P. Geng, J. Li, H. Xiao, J. Song, et al., J. Alloys Compd. **831**, 154784 (2020).
20 R. Böhmer, K. L. Ngai, C. A. Angell, and D. J. Plazek, J. Chem. Phys. **99**, 4201 (1993).
21 J. C. Mauro, Y. Yue, A. J. Ellison, P. K. Gupta, and D. C. Allan, Proc. Natl. Acad. Sci. USA **106**, 19780 (2009).
22 I. Echeverria, P. Su, S. L. Simon, and D. J. Plazek, J. Polym. Sci. B Polym. Phys. **33**, 2457 (1995).
23 V. N. Novikov, and A. P. Sokolov, Nature **431**, 961 (2004).
24 W. L. Johnson, J. H. Na, and M. D. Demetriou, Nat. Commun. **7**, 10313 (2016).
25 R. Busch, E. Bakke, and W. L. Johnson, Acta Mater. **46**, 4725 (1998).
26 Y. Zhao, B. Shang, B. Zhang, X. Tong, H. Ke, H. Bai, and W. H. Wang, Sci. Adv. **8**, eabn3623 (2022).
27 J. Orava, and A. L. Greer, J. Chem. Phys. **140**, 214504 (2014).
28 F. W. Cagle Jr., and H. Eyring, J. Appl. Phys. **22**, 771 (1951).
29 H. Eyring, Trans. Faraday Soc. **34**, 41 (1938).
30 L. Song, W. Xu, J. Huo, F. Li, L. M. Wang, M. D. Ediger, and J. Q. Wang, Phys. Rev. Lett. **125**, 135501 (2020).
31 H. W. Starkweather Jr., Macromolecules **14**, 1277 (1981).
32 Q. Yang, S. X. Peng, Z. Wang, and H. B. Yu, Natl. Sci. Rev. **7**, 1896 (2020).
33 J. C. Dyre, Rev. Mod. Phys. **78**, 953 (2006).
34 J. C. Dyre, and W. H. Wang, J. Chem. Phys. **136**, 224108 (2012).
35 K. Takeda, M. Oguni, and H. Suga, Thermochim. Acta **158**, 195 (1990).
36 O. Haida, H. Suga, and S. Seki, Thermochim. Acta **3**, 177 (1972).
37 I. Sugawara, and Y. Tabata, Chem. Phys. Lett. **41**, 357 (1976).
38 L. M. Wang, and R. Richert, J. Phys. Chem. B **111**, 3201 (2007).
39 R. T. Skodje, and D. G. Truhlar, J. Phys. Chem. **85**, 624 (1981).
40 I. R. Sims, Nat. Chem **5**, 734 (2013).
41 V. N. Novikov, and A. P. Sokolov, Phys. Rev. Lett. **110**, 065701 (2013).
42 H. Luan, X. Zhang, H. Ding, F. Zhang, J. H. Luan, Z. B. Jiao, Y. C. Yang, H. Bu, R. Wang, J. Gu, et al., Nat. Commun. **13**, 2183 (2022).
43 Q. Sun, D. M. Miskovic, K. Laws, H. Kong, X. Geng, and M. Ferry, Appl. Surf. Sci. **533**, 147453 (2020).
44 L. Cao, L. J. Song, Y. R. Cao, W. Xu, J. T. Huo, Y. Z. Lv, and J. Q. Wang, Chin. Phys. B **30**, 076103 (2021).
45 Y. Cao, F. Wang, L. Song, M. Li, A. Li, J. Huo, H. Li, F. Li, P. Yu, W. Xu, et al., J. Non-Cryst. Solids **593**, 121764 (2022).
46 F. H. Stillinger, Science **267**, 1935 (1995).
47 A. Thirumalaiswamy, R. A. Riggleman, and J. C. Crocker, Proc. Natl. Acad. Sci. USA **119**, e2210535119 (2022).
48 Y. Yue, Front. Mater. **2**, 54 (2015).
49 A. Q. Tool, J. Am. Ceram. Soc. **29**, 240 (1946).
50 D. J. Plazek, and K. L. Ngai, Macromolecules **24**, 1222 (1991).
51 Q. Zheng, J. C. Mauro, A. J. Ellison, M. Potuzak, and Y. Yue, Phys. Rev. B **83**, 212202 (2011).
52 H. S. Chen, J. Non-Cryst. Solids **27**, 257 (1978).
53 A. Zaccone, J. Phys.-Condens. Matter **32**, 203001 (2020).
54 H. L. Smith, C. W. Li, A. Hoff, G. R. Garrett, D. S. Kim, F. C. Yang, M. S. Lucas, T. Swan-Wood, J. Y. Y. Lin, M. B. Stone, et al., Nat. Phys. **13**, 900 (2017).
55 L. M. Wang, and R. Richert, Phys. Rev. Lett. **99**, 185701 (2007).
56 P. Li, P. Gao, Y. Liu, and L. M. Wang, J. Alloys Compd. **696**, 754 (2017).
57 Y. J. Wang, M. Zhang, L. Liu, S. Ogata, and L. H. Dai, Phys. Rev. B **92**, 174118 (2015).
58 W Meyer, and H Neldel, Z. Tech. Phys. **18**, 588 (1937).
59 Y. Shi, B. Deng, O. Gulbiten, M. Bauchy, Q. Zhou, J. Neuefeind, S. R. Elliott, N. J. Smith, and D. C. Allan, Nat. Commun. **14**, 13 (2023).
60 L. M. Wang, C. A. Angell, and R. Richert, J. Chem. Phys. **125**, 074505 (2006).
61 V. Molinero, S. Sastry, and C. A. Angell, Phys. Rev. Lett. **97**, 075701 (2006).
62 A. S. Manz, M. Aly, and L. J. Kaufman, J. Chem. Phys. **151**, 084501 (2019).
63 H. N. Lee, K. Paeng, S. F. Swallen, and M. D. Ediger, Science **323**, 231 (2009).
64 H. Tanaka, J. Non-Crysta. Solids **351**, 678 (2005).
65 A. Widmer-Cooper, P. Harrowell, and H. Fynewever, Phys. Rev. Lett. **93**, 135701 (2004).
66 C. Zhang, Y. Guo, K. B. Shepard, and R. D. Priestley, J. Phys. Chem. Lett. **4**, 431 (2013).
67 C. M. Roland, S. Hensel-Bielowka, M. Paluch, and R. Casalini, Rep. Prog. Phys. **68**, 1405 (2005).
68 N. Hirai, and H. Eyring, J. Polym. Sci. **37**, 51 (1959).
69 C. H. Reichardt, G. Halsey, and H. Eyring, Text. Res. J. **16**, 382 (1946).
70 H. B. Ke, P. Wen, D. Q. Zhao, and W. H. Wang, Appl. Phys. Lett. **96**, 251902 (2010).